

# Possible role of warm SST bias in the simulation of boreal summer monsoon in SINTEX-F2 coupled model

Susmitha Joseph · A. K. Sahai · B. N. Goswami ·  
Pascal Terray · Sebastian Masson · J.-J. Luo

Received: 10 November 2010 / Accepted: 3 December 2011 / Published online: 23 December 2011  
© Springer-Verlag 2011

**Abstract** Reasonably realistic climatology of atmospheric and oceanic parameters over the Asian monsoon region is a pre-requisite for models used for monsoon studies. The biases in representing these features lead to problems in representing the strength and variability of Indian summer monsoon (ISM). This study attempts to unravel the ability of a state-of-the-art coupled model, SINTEX-F2, in simulating these characteristics of ISM. The coupled model reproduces the precipitation and circulation climatology reasonably well. However, the mean ISM is weaker than observed, as evident from various monsoon indices. A wavenumber–frequency spectrum analysis reveals that the model intraseasonal oscillations are also weaker-than-observed. One possible reason for the weaker-than-observed ISM arises from the warm bias, over the tropical oceans, especially over the equatorial western Indian Ocean, inherent in the model. This warm bias is not

only confined to the surface layers, but also extends through most of the troposphere. As a result of this warm bias, the coupled model has too weak meridional tropospheric temperature gradient to drive a realistic monsoon circulation. This in turn leads to a weakening of the moisture gradient as well as the vertical shear of easterlies required for sustained northward propagation of rain band, resulting in weak monsoon circulation. It is also noted that the recently documented interaction between the interannual and intraseasonal variabilities of ISM through very long breaks (VLBs) is poor in the model. This seems to be related to the inability of the model in simulating the eastward propagating Madden–Julian oscillation during VLBs.

**Keywords** Indian summer monsoon · Intraseasonal oscillations · Interannual variability

---

S. Joseph (✉) · A. K. Sahai · B. N. Goswami  
Indian Institute of Tropical Meteorology,  
Pune 411 008, India  
e-mail: susmitha@tropmet.res.in

A. K. Sahai  
e-mail: sahai@tropmet.res.in

B. N. Goswami  
e-mail: goswami@tropmet.res.in

P. Terray · S. Masson  
LOCEAN, Paris, France  
e-mail: lea@locean-ipsl.upmc.fr

S. Masson  
e-mail: smasson@locean-ipsl.upmc.fr

J.-J. Luo  
RIGC, Yokohama, Japan  
e-mail: luo@jamstec.go.jp

## 1 Introduction

The socio-economic and industrial development in the Indian subcontinent is closely interlaced with the spatio-temporal variability of Indian summer monsoon (ISM). Hence, ISM and its interannual variability (IAV) have always been a topic of research, for more than a century, in the meteorological community. Several attempts have been made in the past using statistical/empirical techniques to improve the seasonal prediction of ISM rainfall (Blanford 1884; Shukla and Mooley 1987; Gowariker et al. 1989, 1991; Goswami and Srividya 1996; Sahai et al. 2003, 2008; Rajeevan et al. 2007, among others). Although statistical models possess reasonable skill in predicting the seasonal mean, they have problems in predicting extreme monsoons and also the monsoon evolution at the regional scale. This

inefficiency of the statistical models makes the state-of-the-art dynamical models, an attractive potential alternative for the prediction of ISM (Kang and Shukla 2006; Xavier and Goswami 2007).

There are several studies in the past that focus on the ability of dynamical models in simulating ISM and its variability. Based on the analysis of a set of atmospheric general circulation models (AGCMs) from the Atmospheric Model Intercomparison Project (AMIP), Sperber and Palmer (1996) found that the models with better rainfall climatology are generally more successful in simulating the IAV of rainfall. Gadgil and Sajani (1998) concluded that most of the AMIP models have problems in simulating the observed monsoon variability and better simulation of IAV is associated with better simulation of the seasonal mean rainfall pattern. They also showed that the realistic simulation of variability in the western Pacific may be useful in simulating the monsoon IAV associated with El-Nino and Southern Oscillation (ENSO). Kang et al. (2002, 2004) suggested that for GCMs to be useful for monsoon studies, it is essential that the main features of the summer monsoon should be simulated by them with reasonable accuracy. In addition, many recent studies (e.g. Wang et al. 2005) argue that coupled GCMs are essential for simulating and predicting the monsoon IAV, as air-sea interaction over the eastern Indian Ocean and Western Pacific warm pool is intrinsic to the annual cycle and IAV of the monsoon.

This has motivated further research using coupled GCMs. Several researchers (e.g., Annamalai et al. 2007; Mandke et al. 2007; Kripalani et al. 2007) analyzed the outputs of a set of coupled GCMs from Intergovernmental Panel on Climate Change (IPCC) Fourth Assessment Report (AR4) project and showed that majority of the models have problems in representing monsoon precipitation climatology and annual cycle realistically. Recently, some studies (Kim et al. 2008; Xavier et al. 2008; Joseph et al. 2010) using the DEMETER (Development of a European Multimodel Ensemble system for seasonal to interannual prediction) coupled models also indicate that the seasonal mean monsoon has not been improved much in these GCMs even after the inclusion of ocean-atmosphere coupled processes.

Thus, the present day AGCMs as well as the coupled GCMs have problems in predicting the seasonal mean monsoon over Indian region with useful skill. Whilst the multi-model ensemble (MME) system shows some improvement over individual models (Krishnamurti et al. 2000, 2001), the over-all performance of the MME system is dependent on the skill of individual models (Joseph et al. 2010; Lee et al. 2011) involved in it. Hence, it is required that the skill of the individual coupled models has to be improved. For this, the biases in the individual models are

to be analyzed in detail. This may provide some direction towards the improvement of the seasonal mean monsoon prediction in the coupled models.

The basic requirement that any model should possess, in order to be used for monsoon studies, is a reasonable climatology of precipitation, circulation and Sea Surface Temperature (SST). The biases in representing these features would lead to problems in representing the ISM variability on intraseasonal and interannual time scales and also its strength. The strength of ISM is closely related to the seasonal migration or the propagation characteristics of the monsoon rain band from the oceanic regions to the continent. During boreal summer, there are three preferred locations of convection over the Asian region (Annamalai and Sperber 2005)—the first one over the Indian subcontinent and over the Bay of Bengal region (hereafter referred as BOB), second over eastern equatorial Indian Ocean (IO), and the third over the warm waters of tropical western Pacific. Within a particular summer monsoon season, the intraseasonal variability (ISV) is characterized by the northward propagation of convection from IO region to BOB, northwestward propagation from western Pacific region to BOB and the eastward propagation along IO and western Pacific region (Lau and Chan 1986; Annamalai and Slingo 2001; Annamalai and Sperber 2005). Hence, in order to simulate the mean ISM and its variability correctly, the dynamical models should represent these three heat sources and their propagation characteristics realistically.

Recently, it has been shown by Joseph et al. (2010) that better simulation of IAV of ISM is dependent on the realistic simulation of the interactions between ISV and IAV. Joseph et al. (2009) showed that this interaction between ISV and IAV occurs through break spells that sustain for more than 10 days (termed as VLBs—very long breaks). They found that 85% of the drought years are associated with VLBs, and hence VLBs are responsible for generating the droughts. It was also shown that all VLBs are associated with an eastward propagating Madden-Julian oscillation (MJO); Madden and Julian (1971, 1994), in the equatorial Indian Ocean and the air-sea interactions on intraseasonal time scales are responsible for the sustenance of break spells and hence droughts. The remaining 15% of the droughts may be generated through external agents like ENSO or the nonlinear interactions between different scales over the monsoon region.

This particular study aims at analyzing the various aspects of mean ISM in a relatively high resolution state-of-the-art coupled ocean-atmosphere GCM. The focus is mainly on the ability/inability of this coupled GCM in simulating the climatological features of ISM, its ISV and the interactions between interannual and intraseasonal variabilities.

The coupled model used in this study is the latest version of SINTEX-F2 (Scale INteraction EXperiment) model. The earlier versions of this model have reasonable precipitation climatology and have been used extensively for ISM studies (Terray et al. 2005; Masson et al. 2005; Cherchi et al. 2007; AjayaMohan et al. 2009), Indian Ocean Dipole (IOD) studies (Gualdi et al. 2003; Fischer et al. 2005) and ENSO related studies (Guilyardi et al. 2003; Luo et al. 2005; Tozuka et al. 2007). Terray et al. (2005) concentrated on the dynamics of ENSO—monsoon relationships in the coupled model, whereas AjayaMohan et al. (2009) examined the role of IOD on the propagation of northward propagating boreal summer ISOs (BSISOs). Guilyardi et al. (2003) analyzed the mechanisms of ENSO phase change using an earlier version of this model. In the present version of the model, some improvements have been made in the physics (refer Sect. 2). Additionally, the atmospheric and oceanic components are changed. Hence, it is worthwhile to examine whether the ISM simulation is improved in the model, compared to its predecessor.

The remaining part of the paper is organized as follows—details of the state-of-the-art coupled model, data used and the methodology adopted are described in Sect. 2; salient features of seasonal mean monsoon and also the reasons for the weaker/better simulation are discussed in Sect. 3; major findings of this study are summarized in Sect. 4.

## 2 Model, data and methodology

The coupled model used in this study is SINTEX-F2, an upgraded version of SINTEX-F1 ocean–atmosphere coupled model (Gualdi et al. 2003; Luo et al. 2003, 2007). The oceanic component of the latest version is NEMO 2.3 (Nucleus for European Modelling of the Ocean; <http://www.loecean-ipsl.upmc.fr/NEMO>) with OPA (acronym for “Océan PARallelisé”; Madec et al. 1998; Madec 2008) for the oceanic dynamical core and LIM2 (Louvain-la-Neuve; Timmermann et al. 2005) for the sea-ice model. We use the configuration known as “ORCA05” which is a tri-polar global grid with  $0.5^\circ \times 0.5^\circ$  resolution. Vertical resolution and mixing are similar to OPA8.2. The atmospheric component is ECHAM5.2 (Roeckner et al. 2003) with a T106 (approximately  $1.125^\circ \times 1.125^\circ$ ) horizontal resolution and 31 hybrid sigma-pressure levels. A mass flux scheme (Tiedtke 1989) is applied for cumulus convection with modifications for penetrative convection according to Nordeng (1994). The coupling information, without any flux correction, is exchanged every 2 h by means of the OASIS-3 coupler (Valcke 2006).

The main technical improvements achieved in the coupled model from SINTEX-F1 to SINTEX-F2 versions are:

- Update of the atmospheric model from ECHAM 4.6 to ECHAM 5.2. Increase the vertical levels from 19 to 31 levels.
- Update of the oceanic model from OPA8 to NEMO: make use of all the new physics of NEMO (partial steps, new TKE, new advection and vorticity schemes) and introduce the sea-ice model LIM2 in the system.
- Redefine the coupling interface to fit with the sea-ice model (now available in NEMO v3.2). Switch from OASIS2.4 to OASIS3 (pseudo-parallel version).

In this study, data of the last 100 years from the 110 year long control simulation called F31 are used.

For the model validation, the following observational and reanalysis datasets have been used: monthly and daily precipitation data from Global Precipitation Climatology Project (GPCP; Adler et al. 2003; Huffman et al. 2001; source—<http://precip.gsfc.nasa.gov/>); gridded daily high resolution ( $1^\circ \times 1^\circ$ ) rainfall data from National Climate Centre, India Meteorological Department (IMD), Pune (Rajeevan et al. 2006); daily circulation, specific humidity and air temperature data from National Center for Environmental Prediction/National Center for Atmospheric Research (NCEP/NCAR) Reanalysis (Kalnay et al. 1996; available at a horizontal resolution of  $2.5^\circ \times 2.5^\circ$  from <http://www.cdc.noaa.gov/>) and NOAA Extended Reconstructed monthly SST (ERSST v2) at a resolution of  $2^\circ \times 2^\circ$  (Smith and Reynolds 2004).

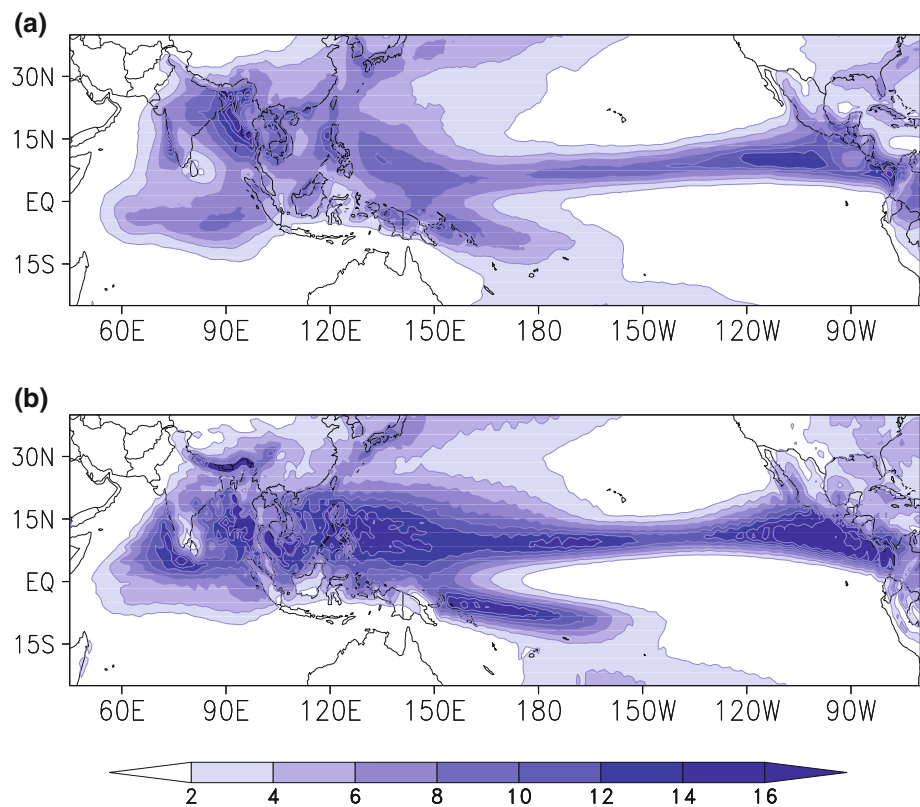
## 3 Results and discussion

This particular study aims at examining the ability of the SINTEX-F2 coupled model in simulating the seasonal and intraseasonal features of ISM. In the first four subsections, the simulated seasonal (JJAS—June to September) mean monsoon is compared with that from the observations. In the following two subsections, the simulation of BSISO and its interaction with IAV are discussed.

### 3.1 Seasonal mean monsoon: precipitation and circulation climatology

Figure 1 depicts the JJAS mean precipitation simulated by the model and its comparison with the observation. The model is able to capture the broader features of ISM. However, it may be noted that the precipitation is over-estimated over the oceanic regions (Fig. 1b). The model is able to reproduce the rainfall along the Head Bay region. It also reproduces the rainfall along the western Pacific region, even though the magnitude is higher-than-observed. The model, however, is unable to reproduce the rainfall maxima over the eastern equatorial IO region. Instead, it

**Fig. 1** Seasonal (JJAS) climatology of precipitation (in  $\text{mm day}^{-1}$ ) for **a** observation, **b** model



produces a maximum over central Indian Ocean region near the southern tip of the peninsular India. The maximum rainfall observed along the west coast of India is slightly dislocated in the model. However, previous version of the model does not exhibit such problem (refer Fig. 1 in AjayaMohan et al. 2009). Thus, among the three heat sources in the Indo-Pacific region, the one over eastern equatorial IO is not correctly simulated by the model. This may have serious implications for the propagation characteristics of ISO of ISM. Another important unrealistic feature is the presence of a rainfall maximum along the foot hills of Himalayas in the model. Earlier versions of the model (Gualdi et al. 2003; Cherchi et al. 2007) also produce the precipitation maxima along the foothills. The same problem is identified for many IPCC AR4 coupled models as well (Annamalai et al. 2007; Mandke et al. 2007). Another bias reported in previous versions of the model is the tendency to produce double ITCZ in the tropical Pacific during boreal summer (Terray et al. 2005). This problem has been resolved to some extent in the present version of SINTEX model (figure not shown).

The JJAS mean atmospheric circulation at upper (200 hPa) and lower (850 hPa) levels, for both observation and model, are shown in Fig. 2. The low-level cross-equatorial flow and the cyclonic vorticity over the BOB region are well simulated by the model (Fig. 2d). However, it has been noticed that the cross equatorial flow is confined

near the Somali coast of Africa in the observations; whereas the flow is all along the equatorial Indian Ocean region in the model. The model captures the upper level easterlies and the anticyclonic circulation over the Tibetan region reasonably well. However, the strength of the upper easterlies is much weaker by about  $5 \text{ ms}^{-1}$  as compared to the observations (Fig. 2b). This could lead to a weak baroclinic structure and would have serious impacts on the northward propagation of BSISO (Jiang et al. 2004). This will be taken up for discussion later on (Sect. 3.7).

### 3.2 Seasonal mean monsoon as indicated by the monsoon indices

Strength of monsoon circulation is often represented by various indices defined from rainfall as well as dynamical parameters. Usage of concise and meaningful indices to characterize monsoon variability could be helpful in assessing the ability of the models in reproducing the variability correctly (Wang and Fan 1999). The choice of indices requires understanding of the essential physics that governs the monsoon variability. In this section, our main objective is to evaluate the simulated ISM circulation using various monsoon indices, defined by earlier researchers.

The All India Monsoon Rainfall (AIMR) Index, defined by the seasonally (JJAS) averaged precipitation all over the Indian subcontinent (Parthasarathy et al. 1992), is a good



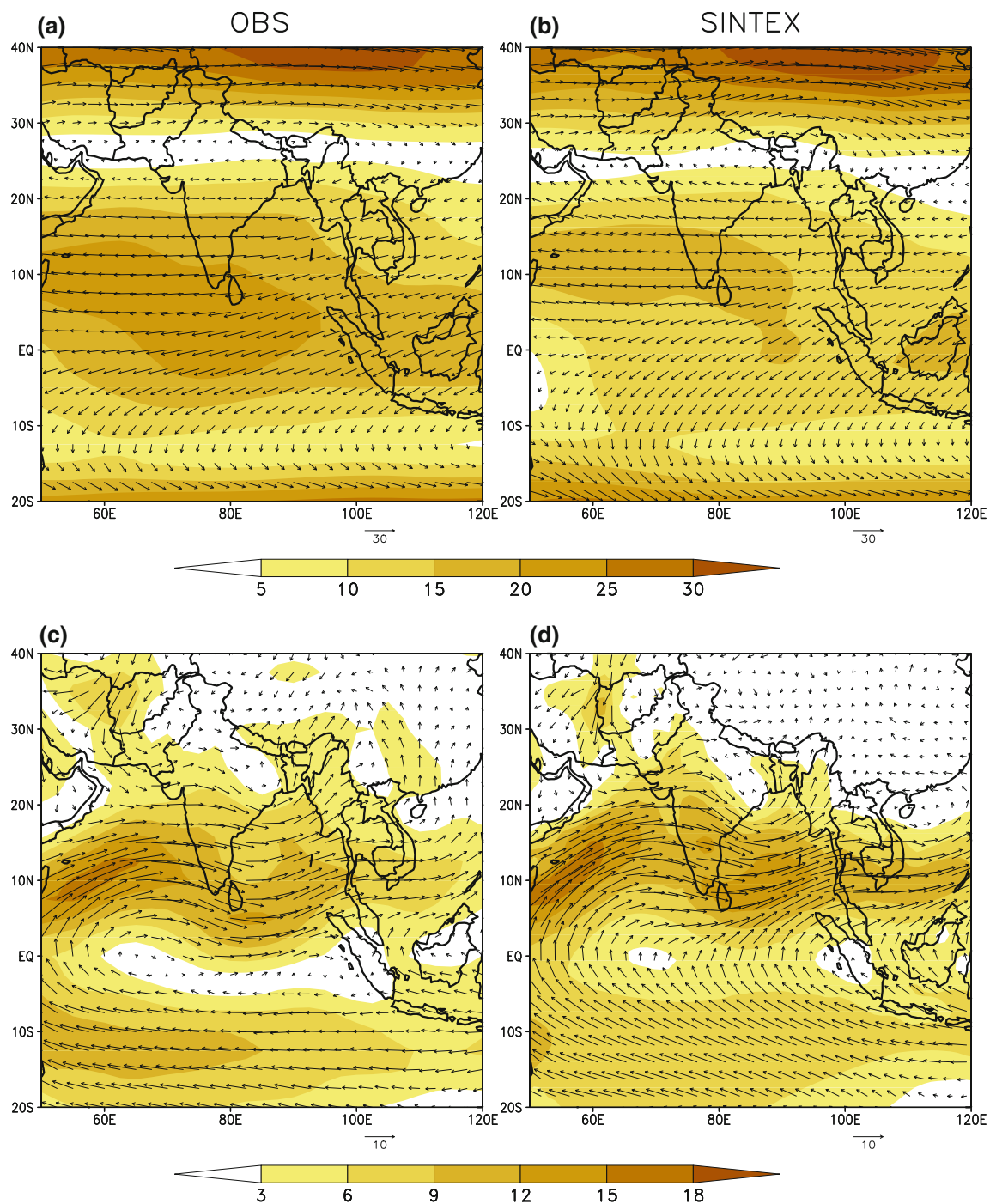


**Fig. 2** JJAS climatology of circulation (in  $\text{ms}^{-1}$ ) at 200 hPa for **a** observation, **b** model, **c** and **d** same as **a** and **b**, but for 850 hPa level. The magnitude of wind is shaded

indicator of the strength of monsoon rainfall over India. The seasonal (JJAS) cumulative rainfall obtained over the Indian subcontinent, defined as Indian Summer Monsoon Rainfall (ISMR), is an excellent measure of ISM. Goswami et al. (1999) introduced an index called Extended Indian Monsoon Rainfall (EIMR) Index from the rainfall averaged over a larger region ( $70^{\circ}$ – $110^{\circ}\text{E}$ ;  $10^{\circ}$ – $30^{\circ}\text{N}$ ), which covers

not only the Indian subcontinent, but also the northern BOB and a portion of South China. They have defined yet another index from the meridional component of wind, which represents the strength of monsoon Hadley circulation, hereafter referred as Monsoon Hadley Circulation (MHC) Index. This is defined by the meridional wind ( $v$ ) shear between 850 and 200 hPa ( $v_{850} - v_{200}$ ) averaged

over the same region as that of EIMR. They have shown that both EIMR and MHC are well correlated with the AIMR. Wang and Fan (1999) defined a circulation index from the meridional shear of zonal wind, i.e., the difference between the westerly anomalies averaged over  $40^{\circ}$ – $80^{\circ}$ E;  $5^{\circ}$ – $15^{\circ}$ N and the westerly anomalies averaged over  $70^{\circ}$ – $90^{\circ}$ E;  $20^{\circ}$ – $30^{\circ}$ N. This index is hereafter referred as WF Index. To reflect the variability of broad scale south Asian summer monsoon, Webster and Yang (1992) used a circulation index (hereafter WY Index), defined by the shear in the zonal component of wind between 850 and 200 hPa ( $u_{850} - u_{200}$ ), averaged over a larger region ( $40^{\circ}$ – $110^{\circ}$ E; equator– $20^{\circ}$ N). WY Index is not much correlated with AIMR (Goswami et al. 1999; Wang and Fan 1999; Annamalai et al. 1999), since WY index describes the large-scale flow, whereas AIMR is based on the regional rainfall pattern. A thermodynamical index based on the tropospheric temperature gradient has been defined by Xavier et al. (2007) to find out the length of monsoon season; hereafter referred as Tropospheric Temperature Gradient (TTG) Index. This is defined by the difference in the tropospheric temperature ( $\Delta$ TT; defined as the temperature averaged between 600 and 200 hPa) between a northern box ( $40^{\circ}$ – $100^{\circ}$ E;  $5^{\circ}$ – $35^{\circ}$ N) and a southern box ( $40^{\circ}$ – $100^{\circ}$ E;  $15^{\circ}$ S– $5^{\circ}$ N). Since positive values of  $\Delta$ TT define the monsoon season, they defined another index called the Thermodynamic Index of Summer Monsoon (TISM) based on the cumulative value of positive  $\Delta$ TT. This index represents the strength of monsoon season and is found to be strongly correlated with AIMR (Xavier et al. 2007). They also defined the length of rainy season (LRS) derived from the positive values of  $\Delta$ TT, i.e., they defined the onset of monsoon season when the value of  $\Delta$ TT becomes positive from negative, and withdrawal of monsoon when  $\Delta$ TT becomes negative from positive and the LRS as the total period when  $\Delta$ TT values are positive.

Table 1 narrates the climatological mean and interannual standard deviation (SD) of the monsoon indices defined above. The values of AIMR and EIMR indicate that the rainfall is more over ocean than over land for the model. The value of MHC index indicates that the shear in the meridional wind is slightly stronger than the observations. This is consistent with the stronger low level and weaker upper level circulation, as explained in Sect. 3.1. The WF index that gives a measure of the strength of monsoon flow is comparatively smaller for the model. Similar is the case with WY index, which represents the baroclinicity of ISM. The TTG index indicates that the meridional gradient of TT is about 30% weak in the model. As a result, TISM and LRS are also less compared to the observations. The ISMR index also signifies that monsoon is weak (by about 15–20%) in the model. Thus, all the monsoon indices are indicative of weaker ISM in the

**Table 1** The climatological mean and interannual standard deviation of various monsoon indices

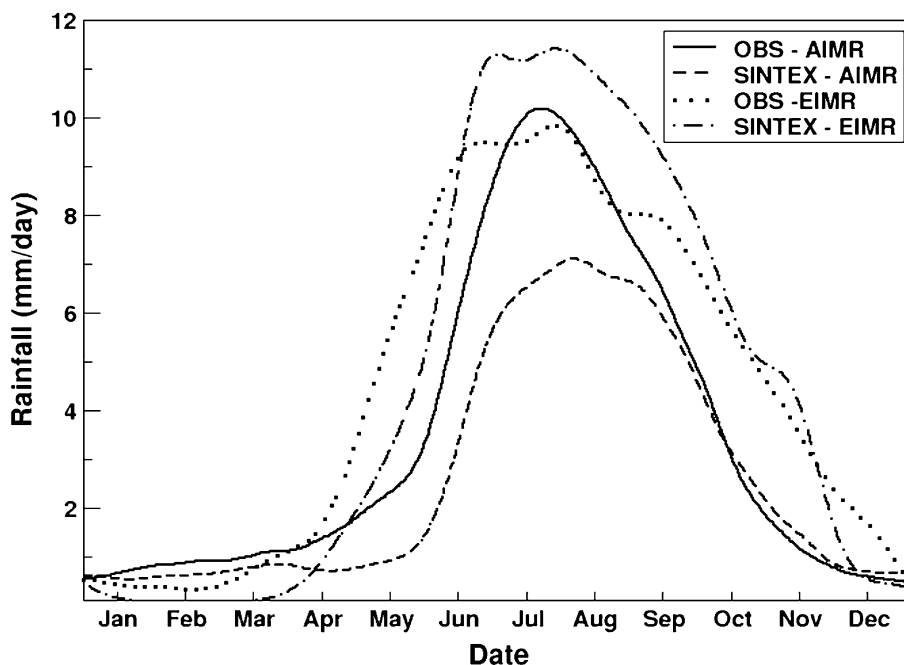
Monsoon indices	Climatological mean (JJAS)	Interannual variability (SD)
AIMR ( $\text{mm day}^{-1}$ )		
OBS	7.753	0.760
SINTEX	5.689	0.674
EIMR ( $\text{mm day}^{-1}$ )		
OBS	8.856	0.669
SINTEX	10.264	0.885
MHC ( $\text{m s}^{-1}$ )		
OBS	4.327	0.380
SINTEX	5.179	0.594
WF ( $\text{m s}^{-1}$ )		
OBS	7.215	0.954
SINTEX	5.801	1.205
WY ( $\text{m s}^{-1}$ )		
OBS	25.409	1.590
SINTEX	20.240	1.777
TTG (K)		
OBS	2.131	0.200
SINTEX	1.428	0.289
TISM (K)		
OBS	266.434	26.906
SINTEX	182.038	32.142
LRS (days)		
OBS	130.533	10.035
SINTEX	110.470	10.845
ISMR (mm)		
OBS	840.74	84.33
SINTEX	691.73	81.98

model. This may be arising from some inherent biases in the model (examined in detail in Sect. 3.7).

### 3.3 Annual cycle

The annual cycle of precipitation is characterized by a sharp increase from April to June and thereafter a gradual decrease from September. Figure 3 depicts the annual cycle of precipitation over Indian subcontinent (AIMR) and over a larger region (EIMR). The figure clearly indicates that intensity of the simulated rainfall is weak over Indian subcontinent (with a deficiency of about  $3 \text{ mm day}^{-1}$  in the peak), but too strong (by about  $2 \text{ mm day}^{-1}$ ) over oceanic region. Over AIMR region, rainfall suddenly increases in the beginning of June, peaks towards the end of July (contrary to mid July in observations) and then continues to decrease till the end of October (similar to observations). The annual cycle of rainfall over

**Fig. 3** Annual cycle of precipitation (in  $\text{mm day}^{-1}$ ) for AIMR region and EIMR region



EIMR region also starts late in the model compared to observations.

### 3.4 Seasonal migration of ITCZ

The northward movement or the seasonal migration of the intertropical convergence zone (ITCZ) during JJAS is illustrated in Fig. 4. Here, the daily precipitation climatology is averaged over the Indian longitudes ( $70^{\circ}$ – $90^{\circ}$ E). From observations, it is clear that precipitation has two maxima, one around  $5^{\circ}$ S and the other around  $20^{\circ}$ N (Fig. 4a). Also, with the beginning of June, ITCZ starts migrating northwards to the Indian latitudes from the oceanic region. In the model, the location of precipitation maxima is displaced. It has two peaks—one around  $5^{\circ}$ N and another around  $30^{\circ}$ N. The peak around  $30^{\circ}$ N is consistent with the maximum precipitation simulated by the model at the foot hills of Himalayas (see Fig. 1b). It is seen from Fig. 4b that ITCZ starts its northward migration by the beginning of June; however, it fails to propagate further northwards and to get established over central India. Thus, the lack of propagation of ITCZ to the northern latitudes may be the reason why the mean rainfall is less over the Indian subcontinent. What is responsible for this lack of propagation is a matter that requires thorough investigation.

### 3.5 Propagation characteristics of ISOs

In the above sections, the climatological features on the seasonal scale were seen. In this subsection, the ability of

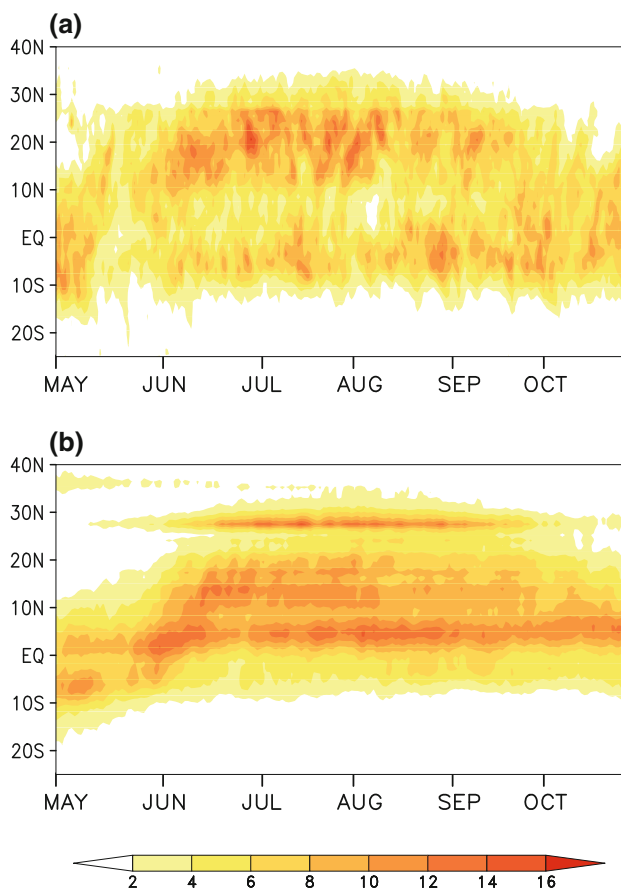


**Fig. 4** Seasonal migration of ITCZ for **a** observation, **b** model

the model in simulating the propagation characteristics of ISOs is addressed. As mentioned earlier, the most significant character of BSISO is its pronounced northward and

eastward propagation of precipitation anomalies from the equatorial IO region.

To examine whether the model simulates the eastward propagating MJO in the equatorial IO region, wavenumber–frequency spectrum analysis (Wheeler and Kiladis 1999), has been performed in the zonal direction over the latitudinal band 15°S–15°N, for the summer season (May to October—MJJASO). While Wheeler and Kiladis (1999) used overlapping 96-day segments to calculate the spectra, Joseph et al. (2009) changed this overlapping 96-day segments by non-overlapping 184-day segments and calculated the spectra. In this study, we have used the methodology of Joseph et al. (2009).

It is evident from Fig. 5 that the model failed to simulate the summer MJO correctly. The spectrum from the observations (Fig. 5a) has maximum power in wavenumber 1. However for SINTEX-F2, the power is considerably less and also the maximum power is spread over a wide range of wavenumbers 1–6, with slightly more power in wavenumber 5 (Fig. 5b). The model is successful to some extent in simulating the boreal winter MJO (figure not shown).

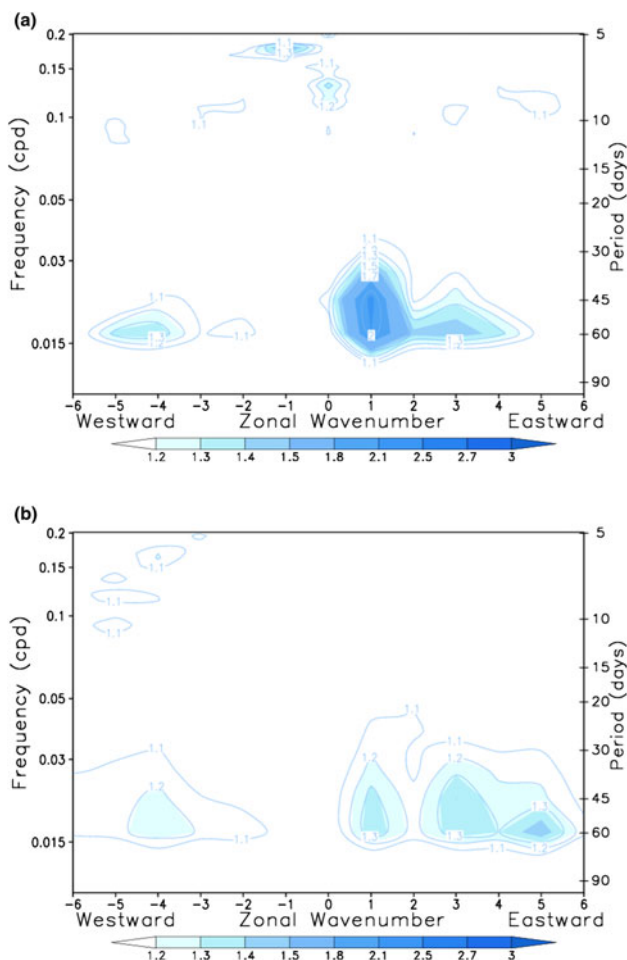


**Fig. 5** Space-time spectra of MJO in the east–west direction for **a** observation, **b** model

However, the wavenumber with maximum power is slightly shifted to higher wavenumber side.

It is evident from the climatological pattern and monsoon indices that the ISM is comparatively weak in the model. The seasonal migration of ITCZ is also not strong in the model. In order to check whether this weakness is reflected in the northward propagating ISOs, wavenumber–frequency spectrum analysis has been carried out, following Wheeler and Kiladis (1999), in the meridional direction. Due care has been taken while performing spectrum analysis for the BSISO, as northward propagating variability is limited to relatively smaller range of latitudes and longitudes, approximately 60°–100°E; 20°S–30°N. Hence, the analysis has been performed over limited domain. Here, meridional wavenumbers are derived for the longitudinal band 65°–95°E. The background spectrum is calculated for the longitudinal band by smoothing the power of spectrum, using a 1-2-1 filter, many times in both frequency and wavenumber, similar to Wheeler and Kiladis (1999). The background spectrum thus calculated is basically found to be red, and has been used to retain the statistically significant spectral peaks. These significant spectra are then plotted. Figure 6 shows the northward propagation for

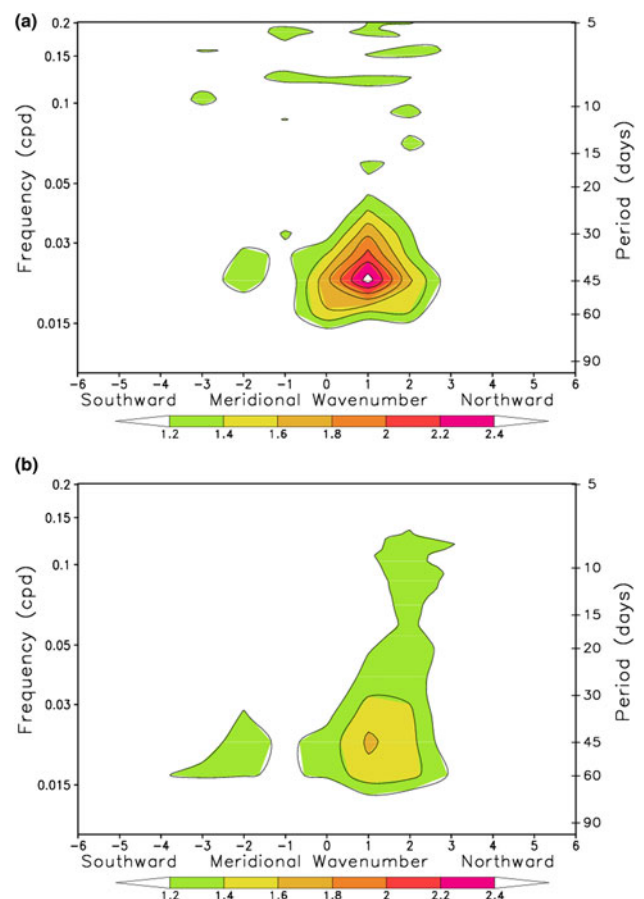


**Fig. 6** Space-time spectra of ISO in the north–south direction for **a** observation, **b** model



observations and model. It is clear from the figure that although the model ISO has maximum power in wavenumber 1 similar to observations, the magnitude is less by about 40%. This poor simulation of ISO propagation in both zonal and meridional directions could lead to problems in simulating the ISV of ISM, as seen in the next subsection.

### 3.6 Interaction between intraseasonal and interannual variabilities through long breaks

In the previous subsections, the ability of the model in reproducing the observed seasonal mean features and propagation characteristics of ISOs has been examined. In this section, we will be analyzing how the model simulates the observed interaction between ISV and IAV. It has been shown by some recent studies (e.g. Joseph et al. 2009; Krishnan et al. 2009) that ISV and IAV interact through long break spells within the monsoon season. Joseph et al. (2009) pointed out the importance of air-sea interaction processes on intraseasonal time scale in the equatorial region, whereas, Krishnan et al. (2009) suggested the role of tropical mid-latitude interactions. Joseph et al. (2009) showed that during very long breaks (VLBs; breaks with duration of more than 10 days), there exists an eastward propagating MJO in the equatorial IO, which may give rise to a divergent field north of the equator. This divergent field may generate Rossby type of wave that moves northwestward towards the Indian region, leading to the sustenance of breaks. Wavenumber—frequency spectrum analysis also confirmed that MJO is dominant in the equatorial region during drought years, similar to the ones observed during winter season over the region. The study also indicated that air-sea interaction on intraseasonal time scale is necessary and sufficient to cause VLBs and hence ISM droughts.

Following Joseph et al. (2009), VLBs have been identified from rainfall data. Break spells were identified when the standardized precipitation anomalies averaged over the central Indian region  $73^{\circ}$ – $82^{\circ}$ E;  $18^{\circ}$ – $28^{\circ}$ N is less than 1.0 for four consecutive days. If the break conditions persist for more than 10 days, they are considered as VLBs. Joseph et al. (2009) indicated that 85% of drought years are associated with VLBs and hence VLBs are responsible for producing ISM droughts. For SINTEX model, out of 100 years, 17 drought years and 8 VLBs occurred. Thus, only  $\sim 40\%$  of drought years are associated with VLBs in the model. This indicates that the model is unsuccessful in reproducing the observed VLB-drought relationship, similar to the CGCMs involved in the DEMETER project (Joseph et al. 2010). The total number of VLBs identified in the coupled simulation is also very less compared to observations. It may be attributed to the fact that active/

break cycles are manifestations of the fluctuations of ITCZ between its continental and oceanic positions in the Indo-Pacific region; and the model has difficulties in reproducing these observed propagation characteristics.

The VLB composite of precipitation anomalies indicate that the model failed to capture the “quadruplet” structure (Annamalai and Slingo 2001; Joseph et al. 2009), with the presence of negative rainfall anomalies over Indian and maritime continents and positive anomalies over equatorial IO and over northwest Pacific (figure not shown). The symmetric pattern of negative and positive rainfall anomalies about the equator (indicating the Kelvin wave dynamics associated with MJO) is also not so clear in the VLB composite. Joseph et al. (2009) demonstrated that during VLBs, there exists an eastward propagating MJO in the equatorial IO, and well organized northward movement of suppressed convection anomalies along the Indian longitudes. The eastward propagating MJO (averaged between  $5^{\circ}$ S and  $5^{\circ}$ N) and northward (averaged between  $70^{\circ}$  and  $90^{\circ}$ E) propagating negative rainfall anomalies are clear in the observations (Fig. 7a, c). The precipitation anomalies are filtered using Lanczos filter (Duchon 1979), to retain the ISO signal (i.e., 20–90 day period band). However, these propagation characteristics during VLBs are not clear in SINTEX-F2 coupled model (Fig. 7b, d). Although some eastward propagation is seen along the equator, the phase speed is not similar to that of MJO. Wavenumber—Frequency spectrum analysis performed during drought years also indicate that the propensity of MJO during these years is not simulated by the model (figure not shown). The model produces maximum power in wavenumbers 4–6, instead of wavenumber 1. It was demonstrated by Joseph et al. (2009) that during VLBs, westerly wind events (WWEs) associated with the MJO initiate air-sea interaction on intraseasonal time scales by extending the warm pool to the east, thus favoring the eastward propagation of MJO further to the east. In order to examine whether the model produces WWEs that are surface signature of MJO, the zonal component of wind at 850 hPa is averaged over the region  $150^{\circ}$ – $170^{\circ}$ E;  $5^{\circ}$ S– $5^{\circ}$ N (Fig. 8). The figure clearly shows that the model failed to capture this particular characteristic of VLBs. Figure 9 depicts that the simulated climatological position of warm pool region, designated by the  $28.5^{\circ}$ C isotherm, extends into the east Pacific, farther east as compared to the observations. This is indicative of an inherent SST warm bias in the model.

### 3.7 Possible reasons for the poor simulation of ISM strength and variability in the model

From the previous sections, it becomes clear that the model has difficulties to simulate the observed characteristics of ISM, its strength and variability. The analysis performed in

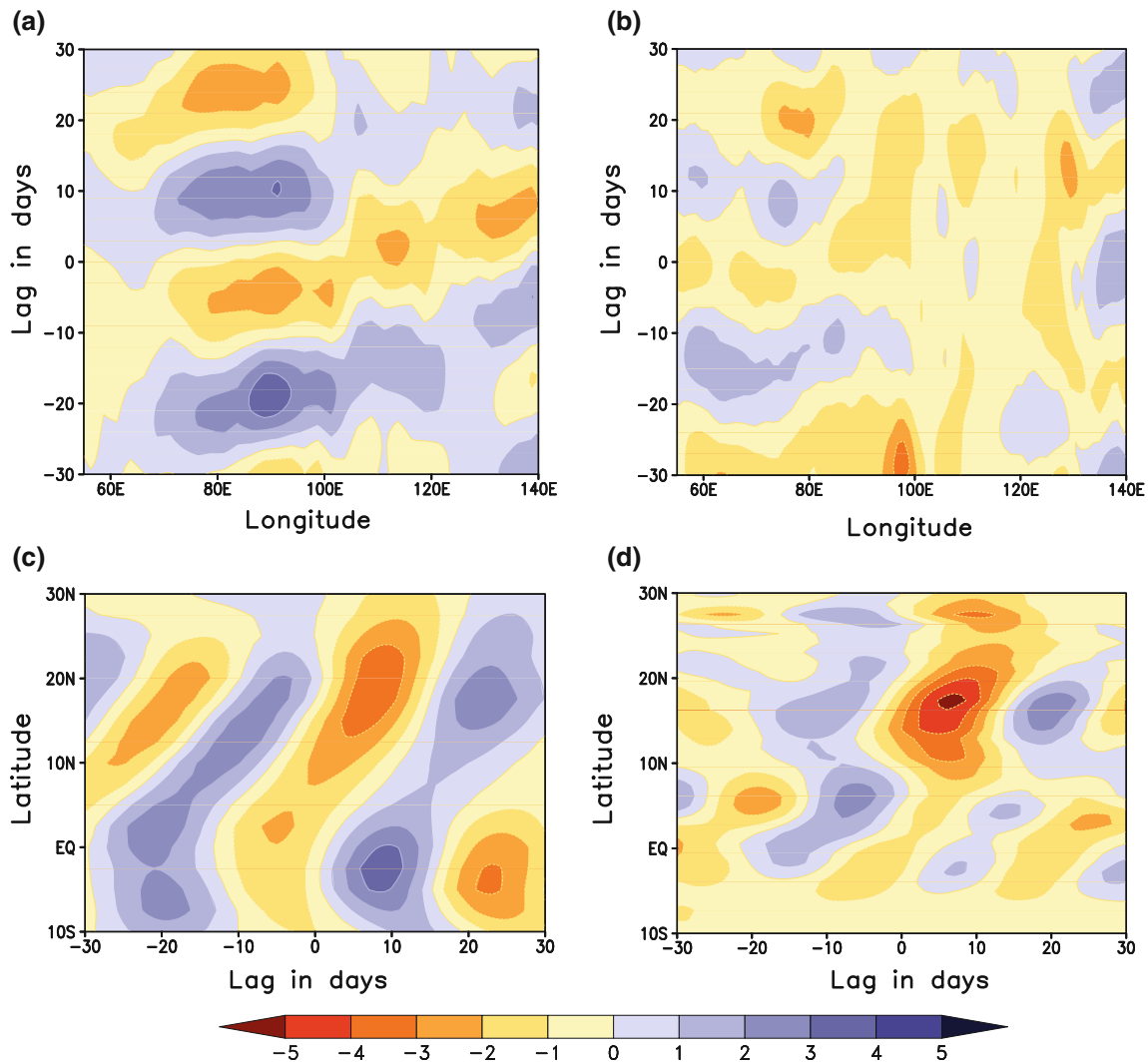


**Fig. 7** Propagation characteristics of 20–90 day filtered rainfall anomalies (in  $\text{mm day}^{-1}$ ) during VLBs **a** along  $5^{\circ}\text{S}$ – $5^{\circ}\text{N}$ , **c**  $70^{\circ}$ – $90^{\circ}\text{E}$ , for observations; **b** and **d** are same as **a** and **c**, but for model. Here, day 0 is the starting day of VLBs

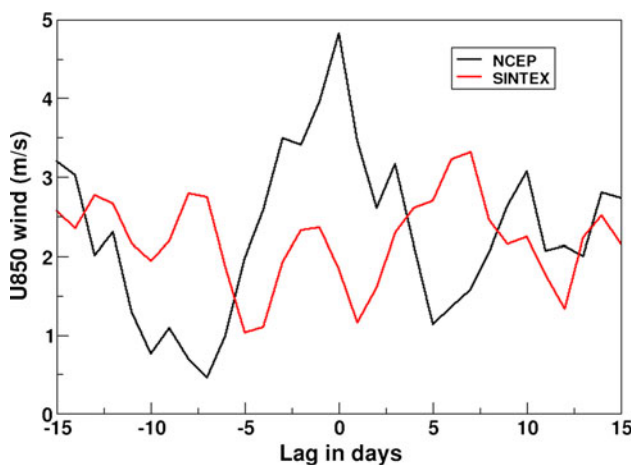


**Fig. 8** VLB composite of zonal wind anomalies in  $\text{m s}^{-1}$  averaged over  $150^{\circ}$ – $170^{\circ}\text{E}$ ;  $5^{\circ}\text{S}$ – $5^{\circ}\text{N}$  for observation and models. Here, day 0 is the starting day of VLBs

the previous sections specifies the following points—less rainfall over the Indian subcontinent, dislocation of the eastern equatorial IO heat source, reduced baroclinic structure indicated by circulation indices and upper air circulation, smaller values of thermodynamic indices, weak propagation characteristics of ISO, especially the northward propagation, poor VLB-drought relationship and warm bias in SST during VLBs. All the above issues pose the following question—whether the model has any inherent bias in simulating the intensity of tropical heat sources correctly?

To answer this question, we have plotted the climatological (JJAS) pattern of SST (Fig. 10). The model has a serious warm bias in simulating the tropical SST pattern, especially over western IO. This would lead to more rainfall than observed over the tropical oceanic regions, as seen in Fig. 1. The JJAS standard deviation of SST

**Fig. 9** Actual SST in degree Celsius during VLBs for **a** observation, **b** model. The climatological position of 28.5°C isotherm is marked as the *black dashed line*

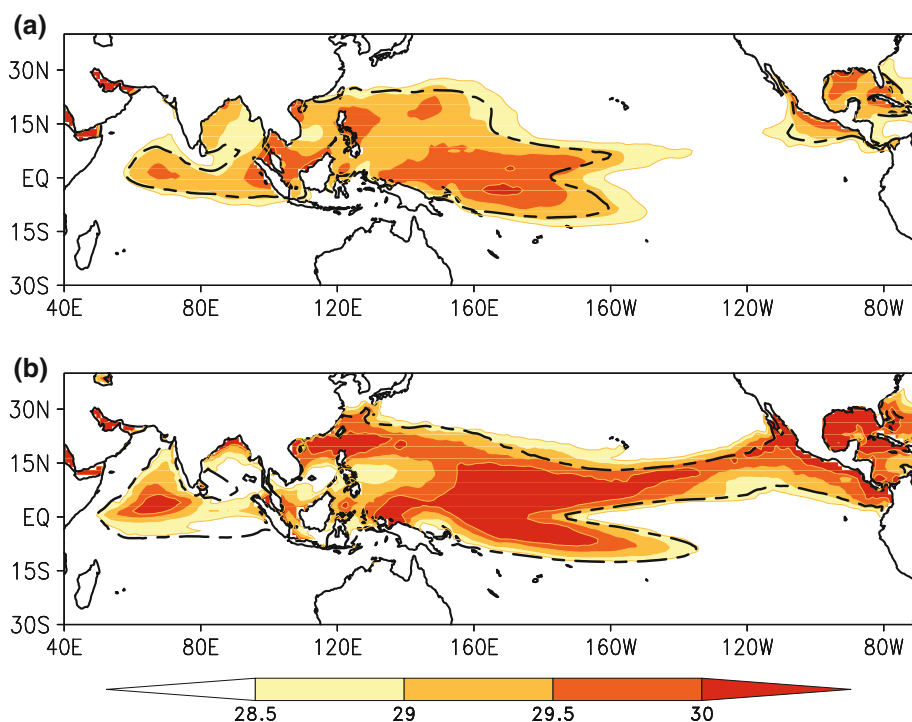
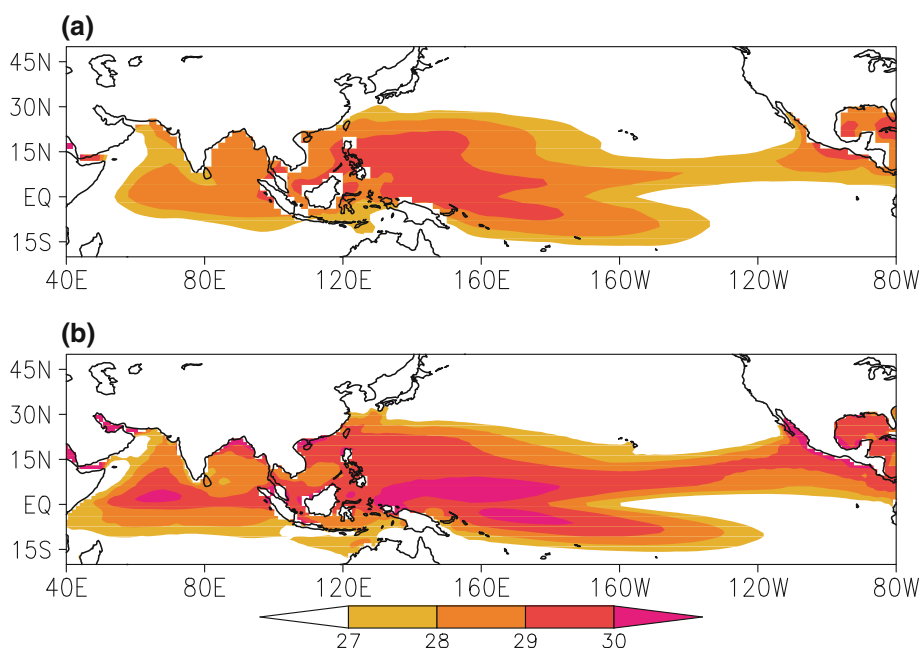


**Fig. 10** JJAS climatology of SST (in °C) for **a** observation, **b** model



illustrates that the model has maximum variability over a broad region covering whole of the equatorial Pacific and over the eastern equatorial IO, off Sumatra coast (figure not shown). On the other hand, the maximum variability is observed only over the eastern equatorial Pacific. Further, it is shown by some earlier studies (e.g., AjayaMohan et al. 2009) that the SINTEX model has a propensity to simulate IOD events. This may be credited to the maximum variance observed over the eastern equatorial IO region.

The tropospheric temperature (TT) plotted during JJAS clearly indicates that the model has a warmer troposphere compared to the observations (figure not shown). The warmer temperatures are observed largely over the tropical oceanic regions. This becomes unambiguous when we plot the TT averaged over the Indian longitudes 65°–95°E, to examine the latitudinal variation (Fig. 11). It is noted that the difference in TT, between the model and observation, is maximum over the oceanic regions, especially to the south

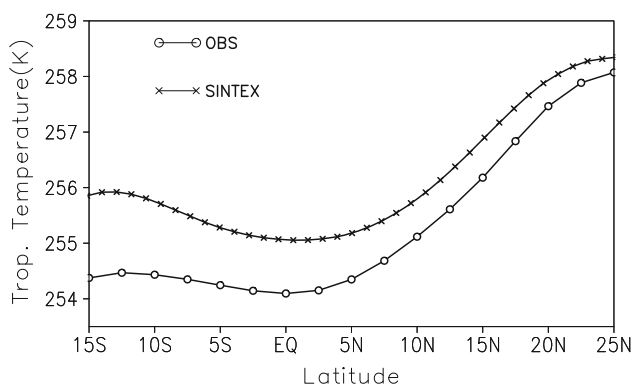


**Fig. 11** Meridional distribution of TT (in K) averaged over 65°–95°E

of the equator. The north–south gradient is about 3.7 K in the observations, whereas, it is only about 2.4 K in the model. This weaker meridional gradient of TT in the model, would lead to weaker TISM and hence weaker ISM (as shown in Table 1 and discussed in Sect. 3.2).

To examine whether the warmer troposphere over the oceanic regions is resulting from the warmer SSTs, we have plotted the vertical profile of air temperature (Fig. 12a) over the region 65°–95°E; 10°S–10°N. It is seen that although the vertical profile of model temperature seems to closely follow the observations, Fig. 12b illustrates that the model is warmer by 1–1.5 K compared to the observations, especially in the middle and upper troposphere. In order to see why the difference in temperature is more in the upper troposphere, we have calculated the vertical advection over the same region (Fig. 12c). The vertical advection in the model increases towards the upper troposphere. Interestingly, vertical distribution of temperature difference between the observation and simulation also exhibits a peak at those levels where the vertical advection in the model is higher (Fig. 12d). Hence, a major part of this difference could be attributed to turbulent mixing through ubiquitous convective activity over the region, which transports the heat upward from the lower layers which are influenced by SST.

Thus, it is suggested that the weak meridional gradient of TT may be resulting from the warm bias inherent in the model over the tropical oceans. In order to examine whether this weakness is reflected in other parameters also, we have plotted the latitudinal variation of specific humidity at 1,000 hPa level, over the longitudinal domain 65°–95°E (Fig. 13). It is noted that the north–south gradient of specific humidity is weak in the model, compared to the observations. Jiang et al. (2004) showed that the meridional gradient of specific humidity and the vertical easterly shear are imperative for the organized northward propagation of ISO. We have also plotted the meridional profile of vertical easterly shear ( $u_{200} - u_{850}$ ) over the same longitudinal band (Fig. 14). It is observed that the easterly shear is

weaker in the model, consistent with strong low level westerlies and weak upper level easterlies (as discussed in Sect. 3.1). It had been noted in Sect. 3.5 that the northward propagation of ISO is weak. This may be due to the insufficient meridional gradient of specific humidity and vertical easterly shear, which in turn arises from the warmer tropical SST. The warmer SSTs may also be responsible for the lack of enhanced migration of ITCZ to the Indian landmass and hence for the reduced precipitation over the subcontinent. The maximum precipitation occurring at around 5°N is probably linked to the misrepresentation of the equatorial heat source; and this has serious implication for the simulation of reverse Hadley circulation associated with monsoon (figure not shown). Indeed, instead of the two preferred locations of convection, one around 5°S and another around 18°N, the model has ascending motion mainly over 5°N.

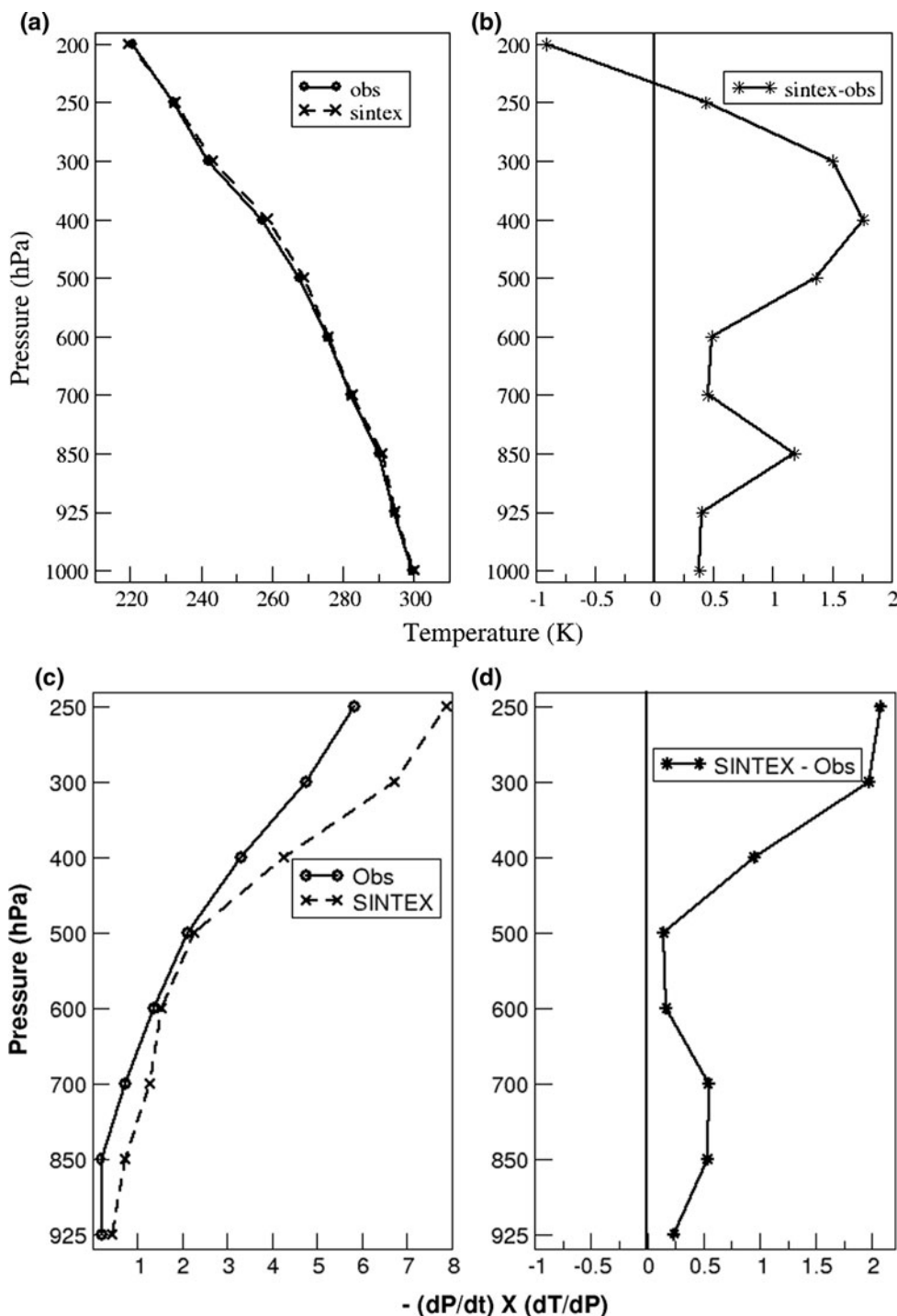
It has been observed that the intraseasonal variability in terms of the occurrence of VLBs is not well captured by the model. It was shown by Joseph et al. (2009) that summer MJO plays a seminal role in generating the VLBs. It has already been shown in Sect. 3.6 that the model failed to capture the propensity of MJO during VLBs. This may be one of the reasons for the poor simulation of VLBs in the model. Even though 7 out of 8 VLBs co-occurred with drought years, most of these (5 out of 8) were associated with El-Nino, giving an indication that these VLBs were being generated not internally, but by the external components of IAV. It has also been demonstrated in Sect. 3.6 that air-sea interaction on intraseasonal timescales, which is imperative for the generation of VLBs, is also not happening in the model.

## 4 Conclusions

In this study, we analyze the ability of SINTEX-F2, a relatively high resolution ocean–atmosphere coupled GCM in simulating the mean features of the ISM, and its variability. We have specifically looked into the following aspects—the simulation of climatological features of ISM, the intensity/strength of monsoon, the propagation characteristics of ISOs and the interaction between ISV and IAV through VLBs.

The analysis reveals that the model has problems in simulating the observed precipitation climatology correctly. The model underestimates the rainfall over Indian subcontinent and overestimates that over the oceanic regions. In the observations, there are two preferred locations of precipitation maxima—one around 5°S and another around 18°N. In the model, the maximum precipitation is seen around 5°N. Due to this, the monsoon Hadley circulation is misrepresented in the model. The strength of monsoon is

**Fig. 12** Vertical distribution of **a** air temperature (in K) for observation and model **b** difference in air temperature (in K) between model and observation, **c** vertical advection (in  $\text{Ks}^{-1}$ ) for observation and model; over the region  $65^{\circ}$ – $95^{\circ}\text{E}$ ;  $10^{\circ}\text{S}$ – $10^{\circ}\text{N}$ , **d** difference in vertical advection (in  $\text{Ks}^{-1}$ ) between model and observation



generally represented by means of various dynamical and thermodynamical indices. Almost all of them indicate that the simulated monsoon is weaker than observed, in the model. It has been noticed that the model captures circulation climatology reasonably well. However, the lower level westerlies are slightly stronger and the upper level easterlies are slightly weaker, compared to the observations, resulting in a weaker vertical easterly shear.

It is worthwhile to note that the model has warm bias in representing the SST in the tropical regions, especially over the equatorial western IO. This warm bias is not only confined to the surface alone, but leads to warming of the whole atmosphere over the equatorial region through sensible and convective mixing processes. This may result in a weak meridional gradient of TT and a weaker monsoon. The weak TT gradient in turn leads to a weak



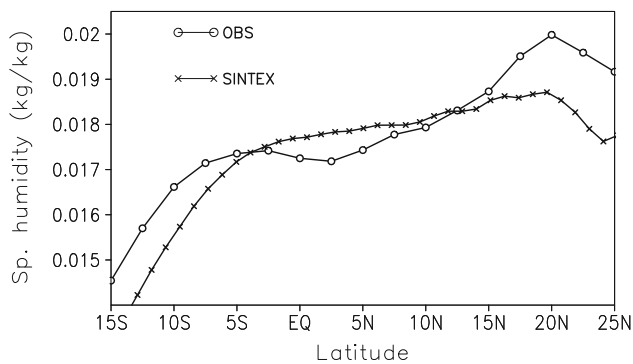


**Fig. 13** Meridional distribution of specific humidity (in  $\text{kg kg}^{-1}$ ) at 1,000 hPa for the longitudinal band  $65^{\circ}$ – $95^{\circ}$ E

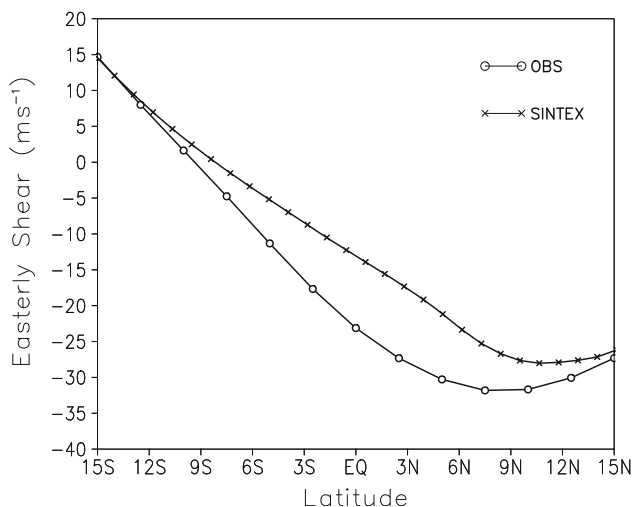


**Fig. 14** Meridional distribution of vertical easterly shear ( $u_{200} - u_{850}$ ; in  $\text{ms}^{-1}$ ) for the longitudinal band  $65^{\circ}$ – $95^{\circ}$ E

meridional distribution of moisture. This may be one of the important reasons why the precipitation maximum is unrealistically simulated around  $5^{\circ}$ N. It may also be responsible for the poor simulation of the northward propagation of ITCZ, or in other words, that of the ISOs, evident from the wavenumber-frequency analysis. The weak vertical easterly shear also plays a vital role in the poor propagation characteristics of ISOs, in the meridional direction. Most of the biases of the model in simulating the seasonal mean monsoon as well as monsoon ISOs thus, seem to stem from the SST bias in the equatorial IO. However, exploring what causes the SST bias is beyond the scope of this particular study. Further analysis is needed to solve this issue.

Many of the ISM biases found in SINTEX-F2 (e.g. less rainfall over the continent and over eastern equatorial IO during boreal summer) are also found in previous versions of this coupled model as documented by Terray et al. (2005), Fischer et al. (2005) and Cherchi et al. (2007).

Such biases are also found in almost all IPCC coupled models (Bollasina and Nigam 2009). These problems must be carefully studied in the future on a model by model basis, and the current work is an initial attempt in this direction. However, it is also worth noting that SINTEX-F2 performs much better than its predecessors for ENSO variability and ENSO-monsoon relationships, thanks to many improvements in the Pacific mean state (Luo et al. 2005; Terray et al. 2011; Masson et al. 2011). In particular, SINTEX-F2 is now able to capture the complex lead-lag relationships between ISM rainfall and monthly Niño3.4 SSTs, while the majority of current state-of-the-art coupled models still fail to reproduce this feature (Terray et al. 2011). This is rather surprising taking into account the deficiencies of the coupled model as far as the Indian Ocean is concerned (see also Terray et al. 2011), but this also suggests that a correct ISM rainfall climatology is not necessarily required for capturing the ISM-ENSO relationship in global coupled models.

Moving to the intraseasonal ISM variability, the VLB-MJO-drought relationship, identified by Joseph et al. (2009) gives useful indication of how ISV and IAV interact with each other. The model failed to reproduce the observed VLB-MJO-drought relationship. It has been demonstrated that the model failed to produce the propensity of MJO during VLBs and the associated air-sea interaction processes on intraseasonal time scale. This may be responsible for the poor simulation of VLBs and its interaction with IAV. It is also worthwhile to note that among the 8 VLBs identified, 7 co-occurred with drought years; and most of them (5 out of 8) were associated with El-Niño, giving an indication that these VLBs were being generated not internally, but by the external components of IAV. However, out of the 17 drought years that occurred during the 100 year period, only 8 were El-Niño years. Hence, it may be believed that the drought years in the model are partly generated by externally varying components of IAV. The rest may be generated through some other mechanisms, like monsoon-midlatitude interactions, as suggested by Krishnan et al. (2009) or through nonlinear scale interactions over the monsoon regions. However, the analysis of these aspects is beyond the scope of the present study.

It is suggested that rectification of the above mentioned deficiencies would potentially improve the simulation of monsoon ISOs and hence the IAV of the ISM in the coupled model. However, the results of this study will be more certain if a parallel fully coupled run with SST bias correction is made with SST strongly nudged to observations. This is an artificial but efficient way to elucidate the possible role of mean SST bias on monsoon and ISO simulations. This issue will be taken as a future work.

**Acknowledgments** This work has been done under the Indo-French project No. 3907/1 entitled “Multi-scale interactions and predictability of the Indian summer monsoon”. IITM is funded by the Ministry of Earth Sciences, Government of India. All experiments were carried out on the Earth Simulator (JAMSTEC) in the frame of the France-Japan collaboration. Special thanks to Dr. K Ashok for help in improving the manuscript.

## References

- Adler RF, Huffman GJ, Chang A, Ferraro R, Xie P, Janowiak J, Rudolf B, Schneider U, Curtis S, Bolvin D, Gruber A, Susskind J, Arkin P, Nelkin E (2003) The version 2 global precipitation climatology project (GPCP) monthly precipitation analysis (1979-present). *J Hydrometeorol* 4:1147–1167
- AjayaMohan RS, Rao SA, Luo J-J, Yamagata T (2009) Influence of Indian Ocean dipole on boreal summer intraseasonal oscillations in a coupled general circulation model. *J Geophys Res* 114:D06119. doi:10.1029/2008JD011096
- Annamalai H, Slingo J (2001) Active/break cycles: diagnosis of the intraseasonal variability over the Asian summer monsoon. *Clim Dyn* 18:85–102
- Annamalai H, Sperber KR (2005) Regional heat sources and the active and break phases of boreal summer intraseasonal (30–50 day) variability. *J Atmos Sci* 62:2726–2748
- Annamalai H, Slingo JM, Sperber KR, Hodges K (1999) The mean evolution and variability of the Asian summer monsoon: comparison of ECMWF and NCEP–NCAR reanalyses. *Mon Weather Rev* 127:1157–1186
- Annamalai H, Hamilton K, Sperber KR (2007) The South Asian summer monsoon and its relationship with ENSO in the IPCC AR4 simulations. *J Clim* 20:1071–1092
- Blanford HF (1884) On the connection of the Himalaya snowfall with dry winds and seasons of drought in India. *Proc R Soc Lond* 37:3–22
- Bollasina M, Nigam S (2009) Indian Ocean SST, evaporation, and precipitation during the South Asian summer monsoon in IPCCAR4 coupled simulations. *Clim Dyn* 33:1017–1032. doi:10.1007/s00382-008-0477-4
- Cherchi A, Gualdi S, Behera SK, Luo J-J, Masson S, Yamagata T, Navarra A (2007) The influence of Tropical Indian Ocean SST on the Indian summer monsoon. *J Clim* 20:3083–3105. doi:10.1175/JCLI4161.1
- Duchon CE (1979) Lanczos filtering in one and two dimensions. *J Appl Meteorol* 18:1016–1022
- Fischer AS, Terray P, Guilyardi E, Gualdi S, Delecluse P (2005) Two independent triggers for the Indian Ocean Dipole/zonal mode in a coupled GCM. *J Clim* 18:3428–3449
- Gadgil S, Sajani S (1998) Monsoon precipitation in the AMIP runs. *Clim Dyn* 14:659–689
- Goswami P, Srividya (1996) A novel neural network design for long-range prediction of rainfall pattern. *Curr Sci* 70:447–457
- Goswami BN, Annamalai H, Krishnamurthy V (1999) A broad scale circulation index for interannual variability of the Indian summer monsoon. *Q J R Meteorol Soc* 125:611–633
- Gowariker V, Thapliyal V, Sarker RP, Mandal GS, Sikka DR (1989) Parametric and power regression models: new approach to long range forecasting of monsoon rain in India. *Mausam* 40:125–130
- Gowariker V, Thapliyal V, Kulshrestha SM, Mandal GS, Sen Roy N, Sikka DR (1991) A power regression model for long-range forecast of southwest monsoon rainfall over India. *Mausam* 42:125–130
- Gualdi S, Guilyardi E, Navarra E, Masina E, Delecluse P (2003) The interannual variability in the tropical Indian Ocean as simulated by a coupled GCM. *Clim Dyn* 20:567–582
- Guilyardi E, Delecluse P, Gualdi S, Navarra A (2003) Mechanisms for ENSO phase change in a coupled GCM. *J Climate* 16:1141–1158
- Huffman GJ, Adler RF, Morrissey M, Bolvin DT, Curtis S, Joyce R, McGavock B, Susskind J (2001) Global precipitation at one-degree daily resolution from multi-satellite observations. *J Hydrometeorol* 2:36–50
- Jiang X, Li T, Wang B (2004) Structures and mechanisms of the northward propagating boreal summer intraseasonal oscillation. *J Clim* 17:1022–1039
- Joseph S, Sahai AK, Goswami BN (2009) Eastward propagating MJO during boreal summer and Indian monsoon droughts. *Clim Dyn* 32:1139–1153. doi:10.1007/s00382-008-0412-8
- Joseph S, Sahai AK, Goswami BN (2010) Boreal summer intraseasonal oscillations and seasonal Indian monsoon prediction in DEMETER coupled models. *Clim Dyn* 35:651–667. doi:10.1007/s00382-009-0635-3
- Kalnay E et al (1996) The NCEP/NCAR 40-year reanalysis project. *Bull Am Meteorol Soc* 77:437–471
- Kang I-S, Shukla J (2006) Dynamic seasonal prediction and predictability of monsoon. In: Wang B (ed) *The Asian monsoon*, chap 15. Springer/Praxis Publishing Co, New York, pp 585–612
- Kang I-S et al (2002) Intercomparison of atmospheric GCM simulated anomalies associated with the 1997–98 El Niño. *J Clim* 15:2791–2805
- Kang I-S, Lee J-Y, Park C-K (2004) Potential predictability of summer mean precipitation in a dynamical seasonal prediction system with systematic error correction. *J Clim* 17:834–844
- Kim H-M, Kang I-S, Wang B, Lee J-Y (2008) Interannual variations of the boreal summer intraseasonal variability predicted by ten atmosphere-ocean coupled models. *Clim Dyn* 30:485–496
- Kripalani RH, Oh JH, Kulkarni A, Sabade SS, Chaudhari HS (2007) South Asian summer monsoon precipitation variability: coupled climate model simulations and projections under IPCC AR4. *Theor Appl Climatol* 90:133–159
- Krishnamurti TN, Kishtawal C, LaRow T, Bachiochi D, Zhang Z, Williford C, Gadgil S, Surendran S (2000) Multimodel superensemble forecasts for weather and seasonal climate. *J Clim* 13:4196–4216
- Krishnamurti TN, Surendran S, Shin DW, Correa-Torres RJ, Vijaya Kumar TSV, Williford E, Kummerow C, Adler RF, Simpson J, Kakar R, Olson WS, Turk FJ (2001) Real-time multianalysis-multimodel superensemble forecasts of precipitation using TRMM and SSM/I products. *Mon Weather Rev* 129:2861–2883
- Krishnan R, Kumar V, Sugi M, Yoshimura J (2009) Internal feedbacks from monsoon–midlatitude interactions during droughts in the Indian summer monsoon. *J Atmos Sci* 66:553–578
- Lau KM, Chan PH (1986) Aspects of the 40–50 day oscillation during the northern summer as inferred from outgoing longwave radiation. *Mon Weather Rev* 114:1354–1367
- Lee DY, Ashok K, Ahn J-B (2011) Toward enhancement of prediction skills of multimodel ensemble seasonal prediction: a climate filter concept. *J Geophys Res* 116:D06116. doi:10.1029/2010JD014610
- Luo J-J, Masson S, Behera S, Delecluse P, Gualdi S, Navarra A, Yamagata T (2003) South Pacific origin of the decadal ENSO-like variation as simulated by a coupled GCM. *Geophys Res Lett* 30(24):2250. doi:10.1029/2003GL018649
- Luo J-J, Masson S, Roeckner E, Madec G, Yamagata T (2005) Reducing climatology bias in an ocean–atmosphere CGCM with improved coupling physics. *J Clim* 18:2344–2360
- Luo J-J, Masson S, Behera S, Yamagata T (2007) Experimental forecasts of Indian Ocean dipole using a coupled OAGCM. *J Clim* 20(10):2178–2190

- Madden RA, Julian PR (1971) Detection of a 40–50 day oscillation in the zonal wind in the tropical Pacific. *J Atmos Sci* 28:702–708
- Madden RA, Julian PR (1994) Observations of the 40–50-day tropical oscillations—a review. *Mon Weather Rev* 122:814–837
- Madec G (2008) NEMO reference manual, ocean dynamics component: NEMO-OPA. Preliminary version. Note du Pole de modélisation, Institut Pierre-Simon Laplace (IPSL), France, No 27 ISSN No 1288-1619
- Madec G, Delecluse P, Imbard M, Lévy C (1998) OPA 8.1 ocean general circulation model reference manual. Note du Pole de modélisation, Institut Pierre-Simon Laplace (IPSL), France, No11, 91 pp
- Mandke SK, Sahai AK, Shinde MA, Joseph S, Chattopadhyay R (2007) Simulated changes in active/break spells during the Indian summer monsoon due to enhanced CO<sub>2</sub> concentrations: assessment from selected coupled atmosphere–ocean global climate models. *Int J Climatol* 27:837–859
- Masson S, Luo J–J, Madec G, Vialard J, Durand F, Gualdi S, Guilyardi E, Behera SK, Delecluse P, Navarra A, Yamagata T (2005) Impact of barrier layer on winter-spring variability of the South-Eastern Arabian Sea. *Geophys Res Lett* 32:L07703. doi: [10.1029/2004GL021980](https://doi.org/10.1029/2004GL021980)
- Masson S, Terray P, Madec G, Luo JJ, Yamagata T, Takahashi K (2011) Impact of intra-daily SST variability on ENSO characteristics in a coupled model. *Clim Dyn*. doi:[10.1007/s00382-011-1247-2](https://doi.org/10.1007/s00382-011-1247-2)
- Nordeng TE (1994) Extended versions of the convective parameterization scheme at ECMWF and their impact on the mean and transient activity of the model in the tropics. Tech. Memo. 206 Eur. Cent. for medium-range weather forecasts, Reading, UK
- Parthasarathy B, Kumar RR, Kothawale DR (1992) Indian summer monsoon rainfall indices: 1871–1990. *Meteorol Mag* 121:174–186
- Rajeevan M, Bhatte J, Kale JD, Lal B (2006) High resolution daily gridded rainfall data for the Indian region: analysis of break and active monsoon spells. *Curr Sci* 91:296–306
- Rajeevan M, Pai DS, Anil Kumar R, Lal B (2007) New statistical models for long-range forecasting of southwest monsoon rainfall over India. *Clim Dyn* 28:813–828
- Roeckner E, Bäuml G, Bonaventura L, Brokopf R, Esch M, Giorgetta M, Hagemann S, Kirchner I, Kornblüeh L, Manzini E, Rhodin A, Schlese U, Schulzweida U, Tompkins A (2003) The atmospheric general circulation model ECHAM 5. PART I: Model description. MPI-report 349
- Sahai AK, Grimm AM, Satyan V, Pant GB (2003) Long-lead Prediction of Indian summer monsoon rainfall from Global SST evolution. *Clim Dyn* 20:855–863
- Sahai AK, Chattopadhyay R, Goswami BN (2008) A SST based large multi-model ensemble forecasting system for Indian summer monsoon rainfall. *Geophys Res Lett*. doi:[10.1029/2008GL035461](https://doi.org/10.1029/2008GL035461)
- Shukla J, Mooley DA (1987) Empirical prediction of the summer monsoon rainfall over India. *Mon Weather Rev* 115:695–704
- Smith TM, Reynolds RW (2004) Improved extended reconstruction of SST (1854–1997). *J Clim* 17:2466–2477
- Sperber KR, Palmer TN (1996) Interannual tropical rainfall variability in general circulation model simulations associated with the atmospheric model intercomparison project. *J Clim* 9:2727–2750
- Terray P, Guilyardi E, Fischer AS, Delecluse P (2005) Dynamics of the Indian monsoon and ENSO relationships in the SINTEX global coupled model. *Clim Dyn* 24:145–168. doi: [10.1007/s00382-004-0479-9](https://doi.org/10.1007/s00382-004-0479-9)
- Terray P, Kamala K, Masson S, Madec G, Sahai AK, Luo JJ (2011) The role of the intra-daily SST variability in the Indian monsoon variability and monsoon-ENSO-IOD relationships in a global coupled model. *Clim Dyn*. doi:[10.1007/s00382-011-1240-9](https://doi.org/10.1007/s00382-011-1240-9) (online)
- Tiedtke M (1989) A comprehensive mass flux scheme for cumulus parameterization in large-scale models. *Mon Weather Rev* 117:1779–1800
- Timmermann R, Goosse H, Madec G, Fichefet T, Ethe C, Duliere V (2005) On the representation of high latitude processes in the ORCA-LIM global coupled sea-ice–ocean model. *Ocean Modell* 8:175–201
- Tozuka T, Luo J–J, Masson S, Yamagata T (2007) Seasonally stratified analysis of simulated ENSO thermodynamics. *J Clim* 20:4615–4627. doi:[10.1175/JCLI4275.1](https://doi.org/10.1175/JCLI4275.1)
- Valcke S (2006) OASIS3 user guide (prism\_2-5). PRISM support initiative report No 3, 64 pp
- Wang B, Fan Z (1999) Choice of South Asian summer monsoon indices. *Bull Am Meteorol Soc* 80:629–638
- Wang B, Ding Q, Fu X, Kang I-S, Jin K, Shukla J, Doblas-Reyes F (2005) Fundamental challenge in simulation and prediction of summer monsoon rainfall. *Geophys Res Lett* 32:L15711. doi: [10.1029/2005GL022734](https://doi.org/10.1029/2005GL022734)
- Webster PJ, Yang S (1992) Monsoon and ENSO: selectively interactive systems. *Q J R Meteorol Soc* 118:877–926
- Wheeler M, Kiladis GN (1999) Convectively coupled equatorial waves: analysis of clouds and temperature in the wavenumber-frequency domain. *J Atmos Sci* 56:374–399
- Xavier PK, Goswami BN (2007) A promising alternative to prediction of seasonal mean all India rainfall. *Curr Sci* 93:195–202
- Xavier PK, Marzin C, Goswami BN (2007) An objective definition of the Indian summer monsoon season and a new perspective on the ENSO–monsoon relationship. *Q J R Meteorol Soc* 133:749–764
- Xavier PK, Duvel JP, Doblas-Reyes FJ (2008) Boreal summer intraseasonal variability in coupled seasonal hindcasts. *J Clim* 21:4477–4497